"Catalytic CVD Synthesis of Double and Triple-walled Carbon Nanotubes by the Control of the Catalyst Preparation"

E. Flahaut*, Ch. Laurent, A. Peigney

CIRIMAT, UMR CNRS-UPS-INPT 5085 / LCMIE, Centre Interuniversitaire de Recherche et d'Ingénierie des Matériaux, Université Paul-Sabatier, 31062 Toulouse Cedex 4, France

(*) Corresponding author:

Dr. Emmanuel Flahaut

CIRIMAT, *UMR CNRS-UPS-INPT 5085* / LCMIE

Bât. 2R1, Université Paul Sabatier

31062 Toulouse Cedex 4 - FRANCE

Tel: +33-5 61 55 69 70

Fax: +33-5 61 55 61 63

E-mail: flahaut@chimie.ups-tlse.fr

"Catalytic CVD Synthesis of Double and Triple-walled Carbon Nanotubes by the Control of the Catalyst Preparation"

E. Flahaut*, Ch. Laurent, A. Peigney

CIRIMAT, UMR CNRS-UPS-INPT 5085 / LCMIE, Centre Interuniversitaire de Recherche et d'Ingénierie des Matériaux, Université Paul-Sabatier, 31062 Toulouse Cedex 4, France

Abstract:

We report the influence of catalyst preparation conditions for the synthesis of carbon nanotubes (CNTs) by catalytic chemical vapour deposition (CCVD). Catalysts were prepared by the combustion route using either urea or citric acid as the fuel. We found that the milder combustion conditions obtained in the case of citric acid can either limit the formation of carbon nanofibres (defined as carbon structures not composed of perfectly co-axial walls or only partially tubular) or increase the selectivity of the CCVD synthesis towards CNTs with fewer walls, depending on the catalyst composition. It is thus for example possible in the same CCVD conditions to prepare (with a catalyst of identical chemical composition) either a sample containing more than 90% double- and triple-walled CNTs, or a sample containing almost 80% double-walled CNTs.

Keywords: A: Carbon nanotubes; B: Catalyst, Catalytic Chemical Vapour Deposition, Combustion; C: Transmission Electron Microscopy.

1. Introduction

The synthesis of carbon nanotubes (CNTs) with a controlled number of walls is an important issue. Most of the work has first focused on single-walled CNTs (SWNTs) because of the extraordinary physical properties expected from the theoretical modelling of their structure. However, when CNTs are to be used in composite materials, the problem of the interface with the matrix becomes crucial, often requiring the functionalisation of the CNT surface. For a SWNT, this corresponds to a degradation of the wall and to possible important modifications of its physical properties. Double-walled CNTs (DWNTs) may be especially interesting since the outer wall would provide an interface with the rest of the system, whereas the structure and properties of the inner tube would remain unchanged. It is thus of fundamental interest to understand how the number of walls can be controlled during the synthesis of the CNTs. The diameter of SWNTs prepared by catalytic chemical vapor deposition (CCVD) is controlled by the diameter of preformed metal particles [1]. In the yarmulke mechanism [1], a graphene cap (the yarmulke) is formed at the surface of the particle and can grow to form a SWNT if the particle is small enough, below *ca*. 3 nm in diameter [2]. A second carbon cap may form underneath the first one, forcing it to lift up and thus forming a DWNT. Using Fe/Mo-Al_2O_3 catalysts prepared by impregnation, Hafner *et al.* [2] reported varying proportions of SWNTs and DWNTs according to the synthesis conditions and noted that there is no correlation between the outer diameter and the number of walls, but that the smallest CNTs (diameter below 1 nm) are never DWNTs. In agreement with the yarmulke mechanism, the present authors reported [3] that, using Fe-Al_2O_3 catalysts with Fe nanoparticles formed *in situ*; DWNTs tend to have a smaller inner diameter than the SWNTs found in the same sample. However, wider inner-diameter distributions for DWNTs and CNTs with three walls (TWNTs) suggested that several base-growth mechanisms may simultaneously operate, depending on the actual characteristics of the catalytic nanoparticle

and also of the temperature, and thus of the supersaturation of the H_2-CH_4 atmosphere which controls the abundance of the carbon source. Increasing the CH_4 content in the atmosphere resulted in an increased number of walls [4]. Cheung *et al.* [5] prepared monodisperse iron particles (3, 9 and 13 nm) on silicon substrate and obtained CNTs with matching diameters (2.6, 7.3 and 11.7 nm, respectively). Interestingly, the number of DWNTs, TWNTs and four-walled CNTs increased with the diameter of the catalytic particles. Zhu *et al.* [6] reported that the relative proportions of SWNTs and DWNTs depended on the nature of the catalytic metal (Fe, Co, or both), its proportion on the substrate, the nature of the substrate (mesoporous silica or zeolite) and reaction conditions such as the temperature, the carbon source and pre-treatments atmosphere.

We have developed $Mg_{1-x}Co_xO$ solid solutions as catalysts for the synthesis of CNTs [7] notably because MgO is then easily removed from the material after the CNTs-forming reaction by a mild non-oxidative washing with an HCl aqueous solution. It was found [7] that more than 80% of the CNTs are either SWNTs or DWNTs (about 50% each) and that more than 90% of all CNTs have a diameter below 3 nm. Several parameters were investigated in order to increase the total yield in CNTs as well as the proportion of DWNTs, including the cobalt content [8] and the preparation route of the starting solid solution [8, 9]. The $Mg_{1-x}Co_xO$ solid solutions were prepared by the nitrate-urea auto-catalytic combustion method [10] using various proportions of fuel (urea) in order to modify the progress of the combustion reaction and eventually the characteristics of the combustion product. Tang *et al.* [11] used basically the same method, however replacing urea by citric acid and adding some molybdenum besides cobalt and magnesium. Using the same treatment for the formation of CNTs as described in our papers [7], these authors reported very high yields of SWNTs, together with the formation of unwanted MWNTs when the Mo:Co ratio was too high. In

contrast with these results, applying the same modifications to our own experiments produced even more DWNTs (ca. 80%) than before [12]. Returning to the use of urea as the fuel, it was found [13] that increasing the Mo:Co ratio leaded to more walls (four-walled tubes at the expense of SWNTs), together with an increase in both the inner and outer diameter, as well as an important increase in the yield. This was in good general agreement with the observations by Tang *et al.* [11], although the total metal loading was not kept constant in their work, which made the comparison difficult. Lyu *et al.* [14] reported that DWNTs with a selectivity estimated to around 90% were produced by catalytic decomposition of *n*-hexane over impregnation-derived Fe/Mo-MgO catalyst. This was mostly attributed to large quantities of highly dispersed catalytic metal particles with a uniform size suitable for the growth of DWNTs.

The present work is focusing on the influence played by the catalyst preparation conditions themselves on the number of walls of the CNTs and shows that a catalyst of a given chemical composition can lead to different products depending on the preparation method used.

2. Experimental

The composition of the main catalyst used for this study is one of those proposed by Tang *et al.* [11]. It can be written $Mg_{0.94}Co_{0.05}Mo_{0.01}O$ by commodity, although the oxide is not a solid solution since molybdenum ions in fact do not enter the MgO rock-salt lattice [13]. The required amounts of $Mg(NO_3)_2.6H_2O$, $Co(NO_3)_2.6H_2O$, and $(NH_4)_6Mo_7O_{24}.4H_2O$ were dissolved in deionised water, together with either urea (catalyst A) or citric acid (catalyst B) as the fuel. This differed from the procedure described by Tang *et al.* [11] who did not dissolve the metal salts, but rather used a limited amount of water. The so-called stoichiometric amount of fuel was calculated [10] and three times that amount was used in the

case of urea, following earlier works [8, 9]. The citric acid amount used was the calculated stoechiometric one. After complete dissolution of the urea (resp. citric acid), the solution was transferred into a crystallising dish and placed in an oven preheated at 550°C, ran with enough air circulation. In the case of urea, the combustion was rather rapid and a flame was visible (observed temperature increase up to at least 650°C). The combustion was over in 5 minutes and the final product (catalyst A) was very light and fluffy, ready to use after only a mild grinding. With citric acid, the progress of the combustion was much less violent and the process was not completed after 15 minutes. No flame was observed and no temperature increase occurred. Some carbon contamination was still present in the combustion product, due to the incomplete decomposition of citric acid and required a calcination in flowing air (2 h, 550°C). The so-obtained product (catalyst B) did not contain any more carbon contamination. Part of sample B was calcined in air at 1000°C for 30 minutes (noted catalyst BC, where C stands for calcined). The catalyst leading to the best quality CNTs was then compared with CNTs prepared using catalysts with a different composition ($Mg_{0.99}Co_{0.0075}Mo_{0.0025}O$) but also prepared by ureic combustion (catalyst D) and by citric acid-combustion [12] (catalyst E).

Each catalyst powder was reduced separately in a H_2-CH_4 atmosphere (18 mol.% CH_4, heating and cooling rates 5°C/min, maximum temperature 1000°C, no dwell) producing CNT-containing composite powders noted A-R, B-R, BC-R, D-R and E-R. These powders were soaked in a concentrated aqueous HCl solution to separate the CNTs by dissolving all the remaining oxide material, as well as unprotected metal particles [7, 15]. The acidic suspensions were filtered and washed with deionised water until neutrality. The samples were dried overnight at 80°C in air. The so-obtained CNTs samples are noted CNT-A, CNT-B, CNT-BC, CNT-D and CNT-E, in reference to the starting catalyst.

X-ray diffraction (XRD) patterns of all materials were recorded using Cu-K_α radiation (λ = 0.15418 nm). The carbon content for the composite powders (C_n) and for the corresponding extracted CNTs samples (C_e) was determined by flash combustion with an accuracy of ± 2%. The BET specific surface area of the materials was measured using N_2 adsorption at liquid N_2 temperature in a Micromeritics FlowSorb II 2300 apparatus (the reproducibility of the results is ± 3%). The oxidation of some composite powders was also investigated by thermogravimetric analysis (TGA) in flowing air (heating rate 1°C/min). The composite powders were studied using field-emission-gun scanning electron microscopy (FEG-SEM, Hitachi S4500, operated at 5 kV or 8 kV) and transmission electron microscopy (TEM, JEOL 200CX, operated at 120 kV). Selected CNTs specimens were studied by high-resolution TEM (HRTEM, JEOL 2010, operated at 120 kV). Raman spectra were recorded using a micro-Raman spectrometer (Model XY, Dilor) with back-scattering geometry and at λ = 482.5 nm (less than 1 mW). The samples were placed on a microscope glass slide.

3. Results and discussion

The XRD pattern of catalysts A, B and BC are shown in Figure 1a. The peaks of the rock-salt (Mg, Co)O solid solution are clearly detected. They are much wider for sample B than for sample A, reflecting a lower crystallite size due to the milder combustion in the case of B; XRD pattern of sample B is the noisiest although the scans were all performed in the same conditions. Interestingly, sample BC presents a pattern similar to that of catalyst A. Much smaller peaks (less than 1% of the main peak intensity, not observable in Fig. 1a) were also detected for sample BC, and could correspond to $CoMoO_4$ or to some MoO_x species. This shows that molybdenum species are probably dispersed as small discrete particles at the

surface of the (Mg, Co)O solid solution grains. The microstructure of these samples will be discussed later in the paper. The much higher crystallite size for both A and BC (ca. 100 nm, although A also contains larger grains) was confirmed by FEG-SEM observations (Fig. 2a-c).

The specific surface area (SSA, Table 1) for specimens A and BC is similar (16 and 20 m^2/g, respectively), whereas the value for B is ten times higher (160 m^2/g) in good agreement with the XRD and FEG-SEM data. It is noteworthy that the value for B is close (177 m^2/g) to that reported by Tang *et al.* [11], although their citric acid-combustion process was slightly different as noted above.

The carbon content (C_n) in the composite powders (Table 1) is close to 30 wt.% for A-R and BC-R, and slightly higher (36 wt.%) for B-R. Tang *et al.* [11] estimated 41 wt.% by TGA for a composite powder prepared using a catalyst with the same composition (to be compared to B-R). Note that Tang's sample was cooled down in H_2 alone, instead of the initial H_2-CH_4 mixture, which should decrease the carbon content since flushing CNTs with H_2 at high temperature (1000°C) is known to remove some carbon from the sample and even to open some CNTs [8]. However, the comparison is somehow difficult because the CNTs samples prepared in this study and those described by Tang *et al*. [11] are significantly different.

Table 1: Catalysts prepared by ureic combustion (A, D) or citric acid-combustion (B, BC, E). S_{ss} (m^2/g): specific surface area of the catalyst; C_n (wt.%): carbon content of the corresponding composite powder; C_e (wt.%): carbon content of the corresponding CNTs after elimination of the catalyst; S_e (m^2/g): specific surface area of the CNTs.

Catalyst	**S_{ss} (m^2/g)**	**Composite**	**C_n (wt.%)**	**CNTs**	**C_e (wt.%)**	**S_e (m^2/g)**
A (ureic)	16	(A-R)	30.5	(CNT-A)	90.2	272
B (citric)	160	(B-R)	35.9	(CNT-B)	86.3	574
BC (citric)	20	(BC-R)	30.4	(CNT-BC)	91.7	410
D (ureic)	19	(D-R)	10.8	(CNT-D)	92.4	803
E (citric)	130	(E-R)	13.0	(CNT-E)	89.7	985

The XRD patterns of the composite powders (not shown) show only small differences with the starting catalysts: *fcc*-Co is detected in all samples (although the main *fcc*-Co peak is very weak in the case of BC-R), and Mo_2C is clearly detected only for A-R.

FEG-SEM observation of the composite powders (Fig. 3) reveals a high density of CNTs bundles in all samples. Moreover, carbon nanofibres with diameters up to 40 nm can be observed for sample A-R (Fig. 3a, indicated by black arrows). Much less nanofibres were observed for samples B-R (Fig. 3b, c) and BC-R (Fig. 3d), and CNTs bundles with a maximum diameter close to 50 nm could be mainly seen.

The carbon content (C_e) in the separated CNTs samples (Table 1) is close to 90 wt.% for CNT-A and CNT-BC and slightly lower (86.3 wt.%) for CNT-B. This was confirmed by TGA which also revealed that the carbon oxidation temperature was different for each sample (492°C for CNT-A, 421°C for CNT-B and 460°C for CNT-BC), which could reflect the respective proportion of nanofibres in the specimens, but is also probably in relation with the differences in bundling for these three samples. The presence of disordered carbon in some samples (coatings) could also play a role in the differences observed between the samples.

The comparison of the XRD patterns of the separated CNTs samples (Fig. 1b) gives important information about their composition. In all three samples, a wide peak around 2 $\theta = 25°$ arises from the presence of CNTs and its width can be related to the mean number of walls [16]. This peak is clearly narrower for CNT-A, which could be interpreted as the signature of CNTs with more concentric walls. The next set of three peaks (44.25, 54.57, 75.93°), corresponding to *fcc*-Co, was especially marked for CNT-A and CNT-B. It is worth noting that these peaks are wider for CNT-B than for CNT-A, indicating smaller particles in the case of CNT-B. These peaks are more difficult to distinguish clearly for CNT-BC. All the other peaks come from Mo_2C and η-Mo_3C_2, although the presence of some η-MoC could not

be ruled out in the case of CNT-A. It is important to note that these peaks are much less intense for CNT-BC and notably CNT-B. These differences will be discussed later in the paper.

The SSA of the separated CNTs samples (S_e, Table 1) is rather low for CNT-A (272 m^2/g), much higher for CNT-B (574 m^2/g) and is in between for CNT-BC (410 m^2/g). This is again in good agreement with the different proportions of carbon nanofibres because we have shown [17] that the SSA of CNTs decreases sharply when the number of walls and the diameter increases. Because carbon nanofibres have wider diameters and much more carbon walls than CNTs, the more they are present in a sample, the lower the SSA. The SSA of the CNTs samples obtained by Tang *et al.* [11] was 704 m^2/g, but this could reflect some opening of the CNTs during the cooling down step performed by these authors in pure H_2 and also the use of a strong oxidising acidic washing (concentrated HNO_3 instead of HCl).

All CNTs samples were characterised by Raman spectroscopy (Fig. 4). In the high-frequency region (Fig. 4a), the ratio between the intensity of the D band (at 1350 cm^{-1}) and the G band (close to 1580 cm^{-1}), noted $I_{D/G}$, is compared. $I_{D/G}$ is similar for CNT-A and CNT-BC (60 and 50 %, respectively) while it is significantly lower for CNT-B (11%). An increasing $I_{D/G}$ value corresponds to a higher proportion of sp^3-like carbon, which is generally attributed to the presence of more structural defects. This could reflect here the proportion of nanofibres. The G band frequency and line-width was similar for all three samples (spectra recorded in the same conditions). In the case of CNT-B, the G band could be fitted by a combination of two Lorentzian-shape curves (around 1552 cm^{-1} and 1576 cm^{-1} respectively). The radial breathing modes (RBM) are observed in the low-frequency region of the spectra (Fig. 4b). No RBM peaks are detected for CNT-A, a few peaks are observed for CNT-BC and much more intense peaks are detected for CNT-B. The diameter distribution calculated from the frequency of the RBM peaks [18] is ranging between 1 and 2.5 nm. It must be kept in mind

that the Raman process is influenced by optical resonance. It is thus not possible with only one wavelength (482.5 nm) to scan the whole population of CNTs present within a sample, because a specific excitation wavelength enhances the signal for only some of the CNTs. Moreover, RBM peaks cannot be observed for too low wave-numbers and this limits the observation range to a maximum diameter of about 3 nm. For CNT-B and CNT-BC, two pairs of peaks are observed in each sample (122.3 and 209 cm^{-1}; 160 and 288 cm^{-1} for CNT-B and 111 and 158 cm^{-1};136 and 220 cm^{-1} for sample CNT-BC), which both correspond to a diameter difference close to 0.7 nm. This could be interpreted as the outer and inner diameter of DWNTs [13, 19].

TEM observations of the separated CNTs specimens (Fig. 5) are in general agreement with the above results. CNT-A (Fig. 5a) was found to contain an important amount of carbon nanofibres (pointed by dark arrows); CNT-B (Fig. 5b) and CNT-BC (Fig. 5c) are rather similar, although the proportion of carbon nanofibres (pointed by dark arrows) was found to be higher in CNT-BC. Figure 6(a) shows some high-resolution images of typical carbon nanofibres. Figure 5(a) also reveals that carbon-encapsulated cobalt or molybdenum carbide nanoparticles (diameter up to 20 nm) are present in CNT-A. This is a *post mortem* evidence of the heterogeneity of the starting catalyst [7, 15] since such particles are formed more easily if the parent oxide particles are larger or poorly dispersed. Figure 5(b) shows some of the rare carbon nanofibres found in sample CNT-B, supported over a bundle of CNTs. Only very small metal or carbide particles were observed in CNT-B. For CNT-BC, all the observed particles were included in carbon nanofibres, or found at the tip of some of the largest CNTs. In all three cases, most CNTs were closed and often contained a particle at their tip.

Catalyst A was prepared by ureic-combustion, which proved to be more violent that the citric acid-combustion used for catalyst B, and thus likely to be more heterogeneous. This

probably implies that the dispersion of molybdenum is worse in catalyst A, which could then favour the formation of molybdenum carbides. Heterogeneity of the distribution of molybdenum may limit the interactions of this element with cobalt and favour the growth and coalescence of larger cobalt particles. These larger metal particles are known to favour the formation of carbon nanofibres. If one now compares catalysts B and BC, it is obvious from the XRD and SEM data that the air calcination at 1000°C has leaded to grain growth and partial sintering of the oxide. This could then explain the formation of larger molybdenum oxide particles in catalyst BC. Catalyst B has a SSA of 160 m^2/g even after a 2-hour calcination in air at 550°C. This means on the one hand that no crystallite growth can be expected lower than this temperature during the CCVD. On the other hand, this must be compared to the ten times lower SSA of catalyst BC which contains larger oxide particles, likely to promote the formation of larger metal particles at a temperature lower than 550°C. The last comparison between catalysts A and BC shows that the homogeneity of the starting oxide is probably the most important parameter since they both have a similar microstructure and specific surface area, but however lead to very different products: mainly carbon nanofibres for catalyst A, mainly CNTs in the case of catalyst BC. It is thus important to work with a catalyst as homogeneous as possible. The role of molybdenum seems to be mainly to promote the decomposition of CH_4 in the case of catalysts A and BC, with probably no alloy effect between Co and Mo. In the case of catalyst B, the mechanism may be different and the very low amount of molybdenum carbide found in B-R and CNT-B (Fig. 1b) could suggest the formation of an alloy between Co and Mo, although we have no direct evidence to confirm this hypothesis.

In contrast with the urea combustion, the citric acid combustion proceeds at lower temperature and takes longer, which seems to favour a better dispersion of the cobalt and molybdenum species. During the heating ramp at the beginning of the CCVD, catalytic

nanoparticles are formed first, by reduction of cobalt and molybdenum species. Previous results [13] have indicated that in our CCVD conditions free molybdenum enhances the decomposition of CH_4 so much that this leads to the formation of carbon nanofibres. However that may be, the question of the exact composition of each catalyst at the beginning of the CCVD may also be important, especially for catalysts A and BC because MoO_3 is significantly volatile at a temperature higher than around 600°C, a temperature which has been reached for both catalysts at some point during their preparation. However, XRD patterns of the corresponding CNTs samples has clearly shown that these two samples contained molybdenum carbides, and a lot more than the CNTs prepared from catalyst B (maximum temperature preparation: 550°C). It thus seems that no significant amount of molybdenum was lost during the catalyst preparation even if the temperature was higher than 600°C.

The formation of thin CNTs will be favoured by an homogeneous population of small enough catalytic particles, which can only be obtained by reduction of homogeneous oxide catalysts. The more homogeneous catalysts were obtained by the citric acid-combustion. We also know from our previous works that decreasing the total amount of catalytic metal limits or even suppresses the formation of carbon nanofibres (and non-tubular carbon species in general) [8, 20-21]. Of course, the ratio between Co and Mo also plays an important role and the proportion of Mo must be kept as low as possible when the synthesis of CNTs with a low number of walls is desired [13]. We will thus now present in a first time a more in depth characterisation of sample CNT-B. In a second time, we will compare these results to CNTs prepared from two catalysts of identical composition but containing a lower amount of Co and Mo ($Mg_{0.99}Co_{0.0075}Mo_{0.0025}O$), one being prepared by ureic combustion (D) and the other by citric acid-combustion (E).

HRTEM observation of sample CNT-B (see Fig. 6b for examples) allowed the construction of histograms representing the distribution of the number of walls and of the inner and outer diameters for a population of 122 individual CNTs. The sample contained 60% DWNTs and 97% of the CNTs had between 1 and 4 walls (Fig. 7a). The inner diameter was ranging between 0.7 and 5.5 nm and the outer diameter between 1.1 and 6.7 nm (Fig. 7b). Tang *et al.* [11] claimed to have prepared with the same catalyst (same composition, prepared by citric acid-combustion route as well), SWNTs with only a few MWNTs and some amorphous carbon deposits, which is very different from the present results.

Two samples containing less cobalt and molybdenum ($Mg_{0.99}Co_{0.0075}Mo_{0.0025}O$) were prepared either by ureic combustion (catalyst D) or by citric acid-combustion [12] (catalyst E) in the same experimental conditions than catalysts A and B, respectively. They were submitted to the same CCVD treatment to form the CNTs, which were separated by HCl soaking. The separated CNTs were also studied by HRTEM. The main characteristics of these two samples are listed in table 1. The histograms showing the distribution of the number of walls (Fig. 7c, e) and inner and outer diameters (Fig. 7d, f) were established from populations of individual CNTs (133 CNTs for CNT-D and 96 CNTs for CNT-E). The comparison between the distributions of the number of walls shown that there was a clear selectivity towards DWNTs in the case of the citric acid-combustion (CNT-E); the use of urea (CNT-D) resulted in a shift of the whole population to a higher number of walls, mainly DWNTs and TWNTs. This is also linked to the diameter distribution, which was slightly larger for CNT-D (Fig. 7d). The comparison between CNT-B and CNT-E shows that a lower amount of catalytic metals (Co and Mo) in the catalyst results in thinner CNTs with a narrower diameter distribution and the total absence of carbon nanofibres. The comparison between CNT-D and

CNT-E, prepared from the same catalyst composition, gives information about the influence of the catalyst preparation. We have shown that the citric acid combustion leads to even thinner CNTs and strongly enhances the selectivity towards the formation of DWNTs. We think the only difference between these two catalysts comes from their homogeneity. According to the first results presented here, the citric acid-combustion leads to a more homogeneous catalyst, resulting in a more homogeneous population of metal particles during the CCVD, and thus allowing the synthesis of CNTs with both a narrower diameter distribution and fewer walls. We have also shown that this has an important effect on the selectivity towards the number of walls.

4. Conclusion

We have studied the influence of the preparation conditions of different (Mg, Co, Mo)O catalysts on their efficiency to produce CNTs. Catalysts of identical elemental composition but with different amounts of catalytic metals were prepared by the combustion route using either urea or citric acid as the fuel. We have shown that the use of citric acid leads to a milder combustion process occurring at lower temperature, with important consequences for the catalytic properties: the higher specific surface area comes together with a better homogeneity of the catalyst leading to a more homogeneous population of smaller catalytic metal particles and thus to CNTs with fewer walls and lower diameters, as well as a narrower diameter distribution. Replacing urea by citric acid did not improve the yield in CNTs, but only enhanced the selectivity of the catalytic reactions, limiting the formation of carbon nanofibres (in the case of $Mg_{0.94}Co_{0.05}Mo_{0.01}O$) or even favouring the formation of CNTs with fewer walls (in the case of $Mg_{0.99}Co_{0.0075}Mo_{0.0025}O$). With this last catalyst composition, we have shown that modifying the catalyst preparation conditions can lead

either to a mixture of double and triple-walled CNTs (ureic combustion) or to almost 80% DWNTs (citric acid-combustion). This point is very important because the removal of carbon nanofibres or the control of the number of walls of the CNTs is not possible post-synthesis by the purification methods currently available. Although the control of the number of walls of the CNTs during the CCVD synthesis is today still rather empirical, a better knowledge of some of the important steps involved during the formation of the catalytic metal nanoparticles will improve our understanding of the phenomena at work.

Aknowledgements

We acknowledge Lucien Datas from the *Service Commun de Microscopie à Transmission* for his help with TEM and HRTEM observations and the *Groupement Interuniversitaire de Spectroscopie Raman* (both at University Paul Sabatier) for the Raman spectroscopy. E.F. is thankful to Dr R. Almairac and J. Cambedouzou (GDPC, Montpellier University, France) for their help with XRD data analysis.

References

[1] Dai H, Rinzler AG, Nikolaev P, Thess A, Colbert DT, Smalley RE. Single-walled nanotubes produced by metal-catalysed disproportionation of carbon monoxide. Chem. Phys. Lett. 1996; 260: 471-475.

[2] Hafner JH, Bronikowski MJ, Azamian BR, Nikolaev P, Rinzler AG, Colbert DT, Smith KA, Smalley RE. Catalytic growth of single-wall carbon nanotubes from metal particles. Chem. Phys. Lett. 1998; 296: 195-202.

[3] Peigney A, Coquay P, Flahaut E, Vandenberghe RE, De Grave E, Laurent Ch. A study of the formation of single- and double-walled carbon nanotubes by a CVD. J. Phys. Chem. B 2001; 105: 9699-9710

[4] Flahaut E, Peigney A, Laurent Ch. Double-Walled Carbon Nanotubes in Composite Powders. J. Nanosci. Nanotech. 2003; 3: 151-158

[5] Cheung CL, Kurtz A, Park H, Lieber CM. J. Phys. Chem. B. Diameter-Controlled Synthesis of Carbon Nanotubes. 2002; 106: 2429-2433

[6] Zhu J, Yudasaka M, Iijima S. A catalytic chemical vapor deposition synthesis of double-walled carbon nanotubes over metal catalysts supported on a mesoporous material. Chem. Phys. Lett. 2003; 380: 496–502

[7] Flahaut E, Peigney A, Laurent Ch, Rousset A. Synthesis of single-walled carbon nanotube-Co-MgO composite powders and extraction of the nanotubes. J. Mater. Chem. 2000; 10: 249-252

[8] Flahaut E. Synthèse par voie catalytique et caractérisation de composites Nanotubes de carbone – métal – oxyde. Poudres et matériaux denses. Doctoral Thesis, (1999), University Paul Sabatier, Toulouse, France, 229p

[9] Bacsa RR, Laurent Ch, Peigney A, Vaugien Th, Flahaut E, Bacsa WS, Rousset A. J. Am. Ceram. Soc. (Mg,Co)O solid solutions precursors for the large-scale synthesis of carbon nanotubes by catalytic chemical vapor deposition. 2002; 85(11): 2666-2669

[10] Patil KC. Advanced ceramics: combustion synthesis and properties. Bull. Mater. Sci. 1996; 16: 533-541

[11] Tang S, Zhong Z, Xiong Z, Sun L, Liu L, Lin J, Shen ZX, Tan KL. Controlled growth of single-walled carbon nanotubes by catalytic decomposition of CH_4 over Mo/Co/MgO catalysts. Chem. Phys. Lett. 2001; 350: 19-26.

[12] Flahaut E, Bacsa R, Peigney A, Laurent Ch. Gram-Scale CCVD Synthesis of Double-Walled Carbon Nanotubes. Chem. Commun. 2003; 1442-1443

[13] Flahaut E, Peigney A, Bacsa WS, Bacsa RR, Laurent Ch. CCVD synthesis of carbon nanotubes from (Mg, Co, Mo)O catalysts: Influence of the proportions of cobalt and molybdenum. J. Mater. Chem. 2004; 14: 646-653

[14] Lyu SC, Liu BC, Lee SH, Park CY, Kang HK, Yang CW, Lee CJ. Large-Scale Synthesis of High-Quality Double-Walled Carbon Nanotubes by Catalytic Decomposition of n-Hexane. J. Phys. Chem. B. 2004; 108(7): 2192-2194

[15] Flahaut E, Agnoli F, Sloan J, O'Connor C, Green MLH. CCVD Synthesis and Characterization of Cobalt-Encapsulated Nanoparticles. Chem. Mater. 2002; 14: 2553-2558

[16] Cambedouzou J. Les nanotubes de carbone biparois : étude structurale. Private communication

[17] Peigney A, Laurent Ch, Flahaut E, Bacsa R, Rousset A. Specific surface area of carbon nanotubes and bundles of carbon nanotubes. Carbon 2001; 39(4): 507-514

[18] Alvarez L, Righi A, Guillard T, Rols S, Anglaret E, Laplaze D, Sauvajol JL. Resonant Raman study of the structure and electronic properties of single-wall carbon nanotubes. Chem. Phys. Lett. 2000; 316: 186-190

[19] Bacsa R, Peigney A, Laurent Ch, Puech P, Bacsa WS. Chirality of internal metallic and semiconducting carbon nanotubes. Phys. Rev. B 2002; 65: 161404-1 - 161404-4

[20] Flahaut E, Govindaraj A, Peigney A, Laurent Ch, Rousset A, Rao CNR. Synthesis of single-walled carbon nanotubes using binary (Fe, Co, Ni) alloy nanoparticles prepared in situ by the reduction of oxide solid solutions. Chem. Phys. Lett. 1999; 300(1-2): 236-242

[21] Coquay P, De Grave E, Vandenberghe RE, Dauwe C, Flahaut E, Laurent Ch, Peigney A, Rousset A. Mössbauer spectroscopy study of MgAl2O4-matrix nanocomposite powders containing carbon nanotubes and iron-based nanoparticles. Acta Mater. 2000; 48: 3015-3023

FIGURE CAPTIONS

Figure 1: **(a)** X-ray diffraction patterns of the catalysts (A: ureic combustion; B: citric acid-combustion; BC: catalyst B, calcined 30 min. at 1000°C in air); the peaks all correspond to the MgO rocksalt structure. **(b)** X-ray diffraction patterns of the CNTs samples prepared from catalysts A, B and BC (CNT-A, CNT-B and CNT-BC, respectively).

Figure 2: FEG-SEM images of catalysts A (a), B (b) and BC (c).

Figure 3: FEG-SEM images of the composite powders obtained after CCVD at 1000°C: A-R (a), B-R (b, c) and BC-R (d). Black arrows indicate carbon nanofibres.

Figure 4: Raman spectra of the CNTs samples in the high-frequency (a) and low-frequency (b) ranges. The stars (*) indicate possible pairs of peaks corresponding to the inner and outer walls of double-walled CNTs.

Figure 5: TEM images of the CNTs samples: CNT-A (a), CNT-B (b) and CNT-BC (c). Black arrows point to carbon nanofibres.

Figure 6: HRTEM images of typical carbon nanofibres (a) and carbon nanotubes (b) found in samples CNT-A, CNT-B and CNT-BC.

Figure 7: Histograms representing the frequency distribution of the number of walls (a) and diameters (b) for CNT-B; d_i and d_o correspond to the inner and outer diameter, respectively; the elemental composition of the starting catalysts is $Mg_{0.94}Co_{0.05}Mo_{0.01}O$. Histograms comparing the frequency distribution of the number of walls and diameters for CNTs

synthesized with a catalyst prepared by ureic combustion (CNT-D, c and d) or citric acid-combustion (CNT-E, e and f); the elemental composition of the starting catalysts is $Mg_{0.99}Co_{0.0075}Mo_{0.0025}O$.

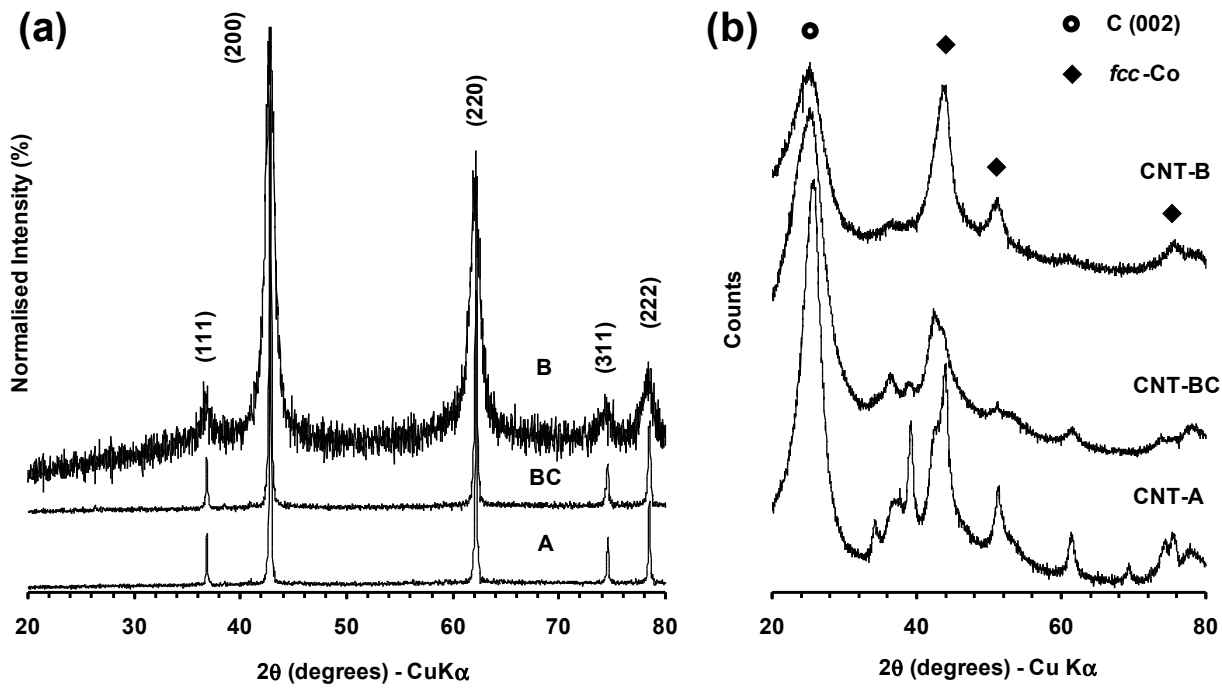
(a)
(200)
(220)
(111)
(311)
(222)
B
BC
A
Normalised Intensity (%)
20
30
40
50
60
70
80
2θ (degrees) - CuKα
(b)
C (002)
fcc-Co
CNT-B
CNT-BC
CNT-A
Counts
20
40
60
80
2θ (degrees) - Cu Kα

FIGURE 1

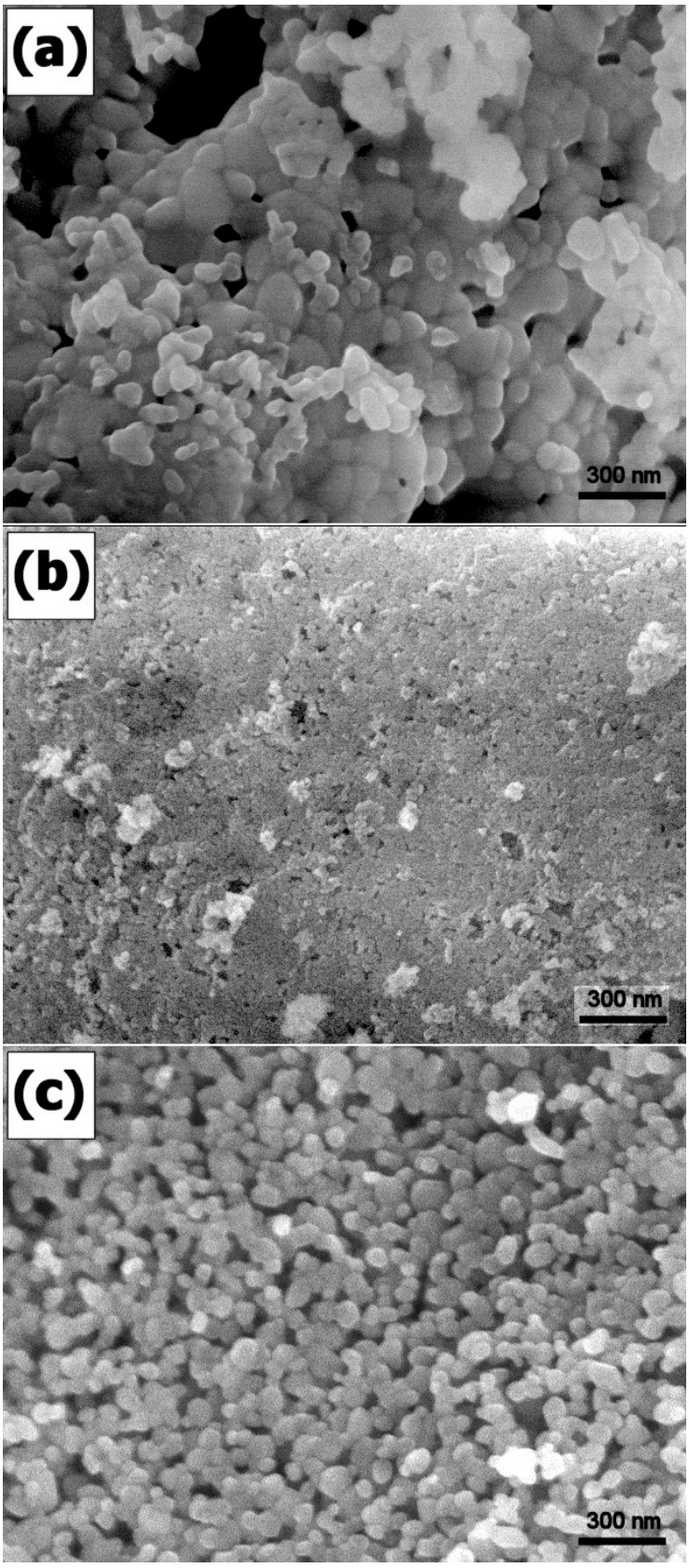

FIGURE 2

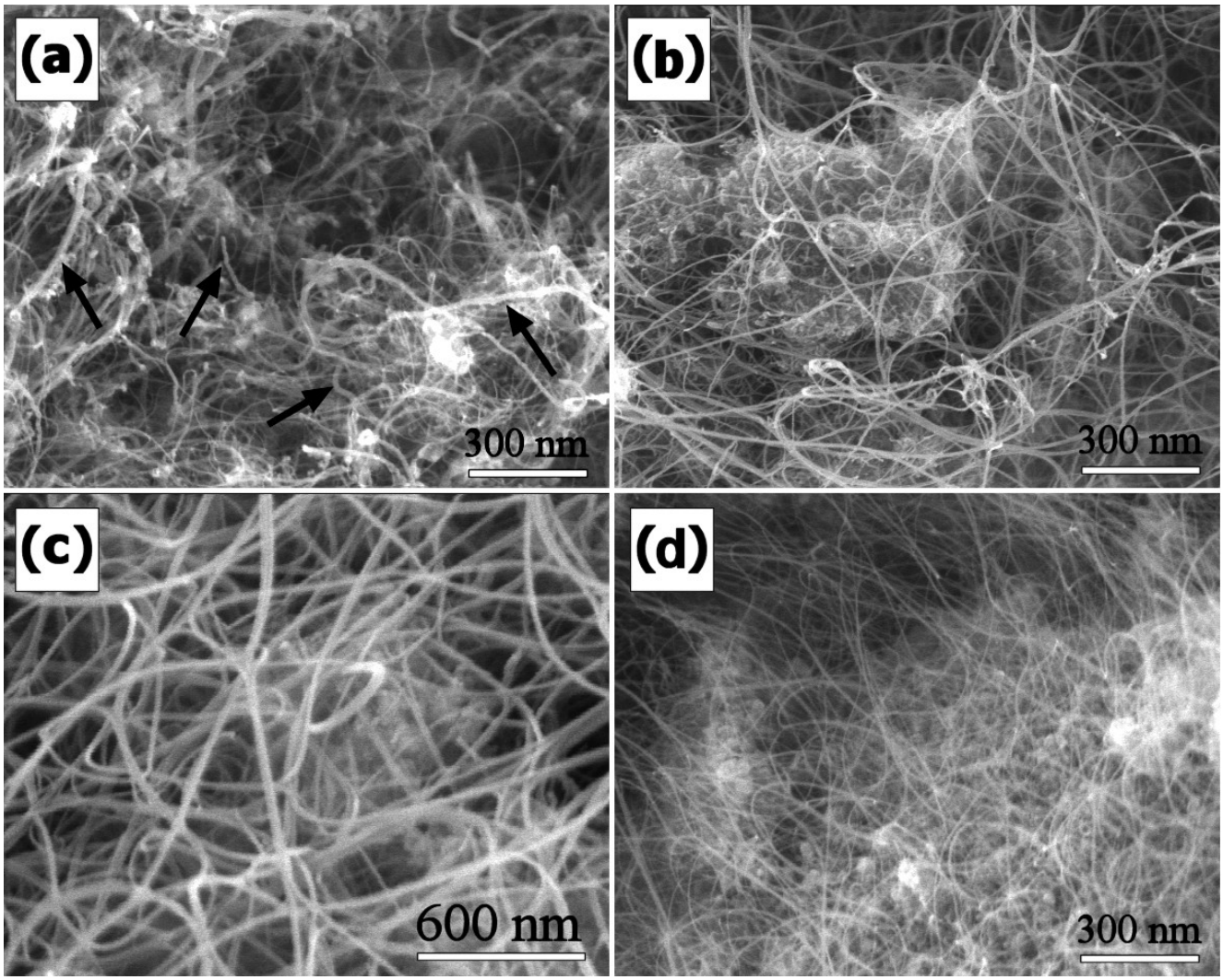

FIGURE 3

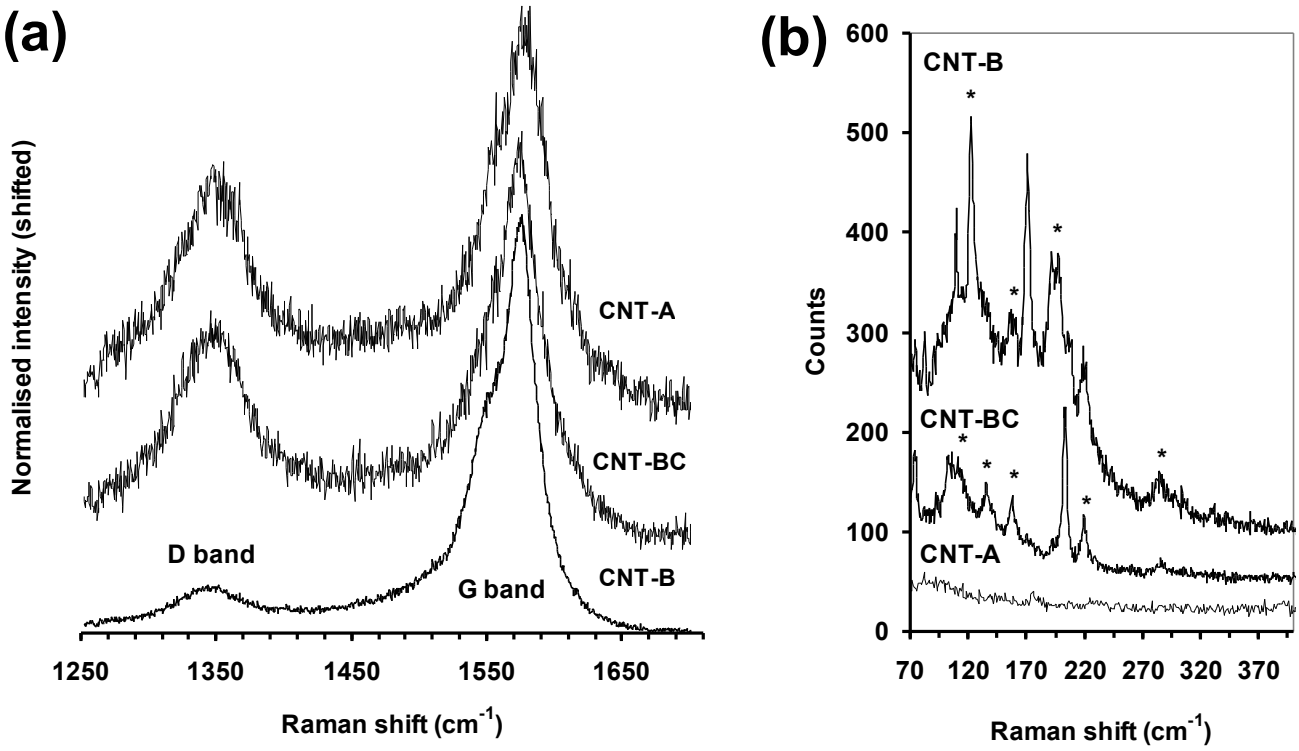
(a)
Normalised intensity (shifted)
CNT-A
CNT-BC
CNT-B
D band
G band
1250
1350
1450
1550
1650
Raman shift (cm-1)
(b)
600
500
400
300
200
100
0
Counts
CNT-B
CNT-BC
CNT-A
70
120
170
220
270
320
370
Raman shift (cm-1)

FIGURE 4

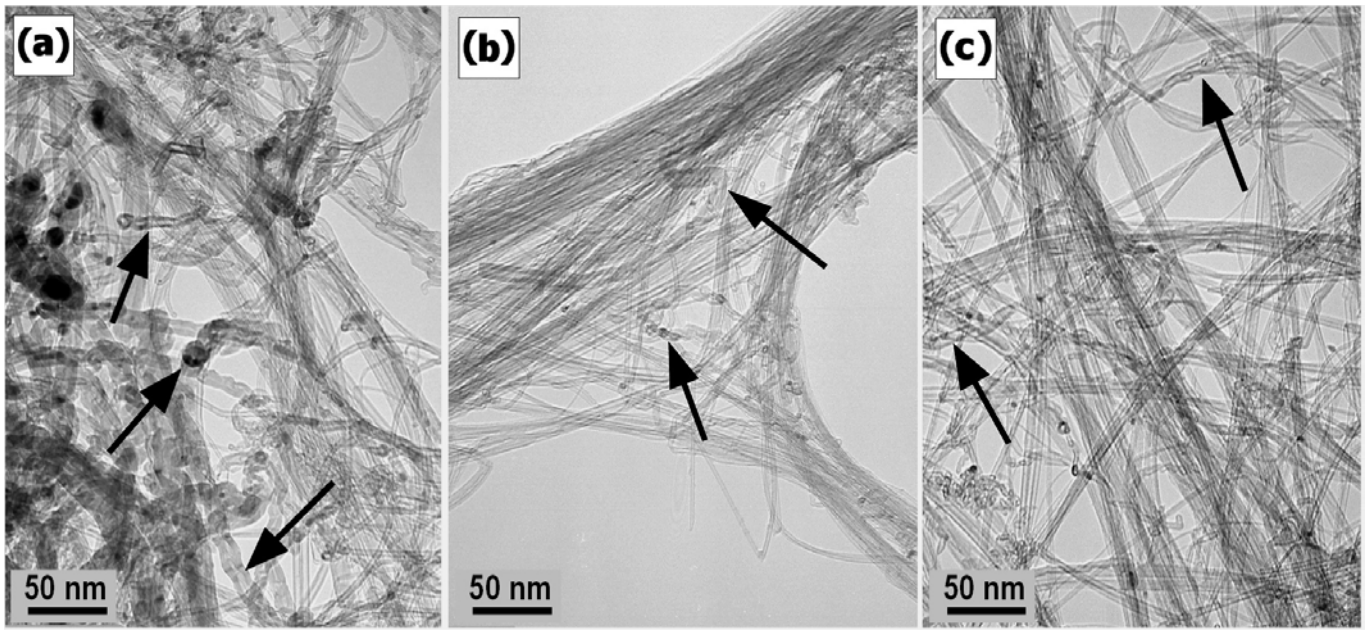

FIGURE 5

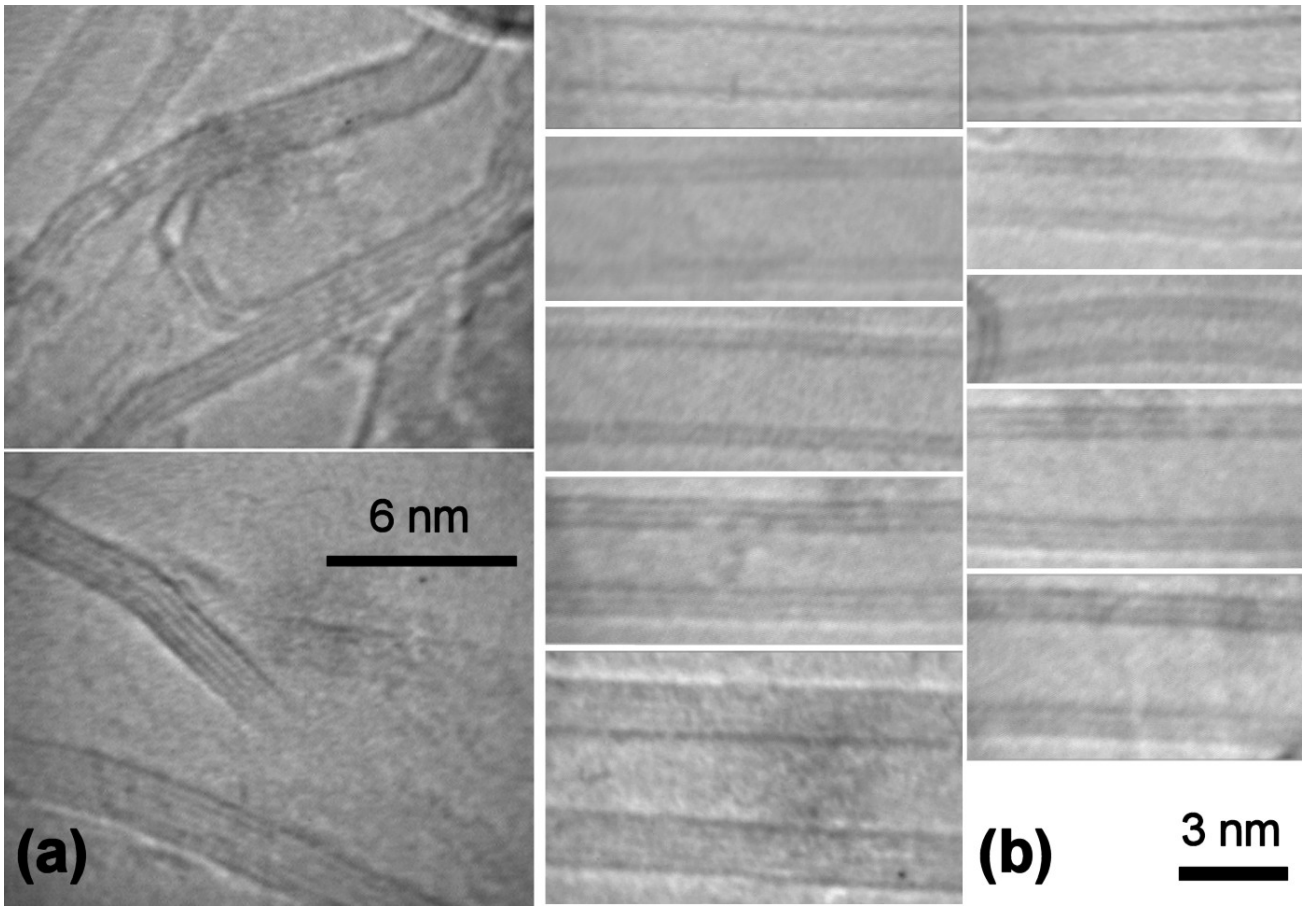

FIGURE 6

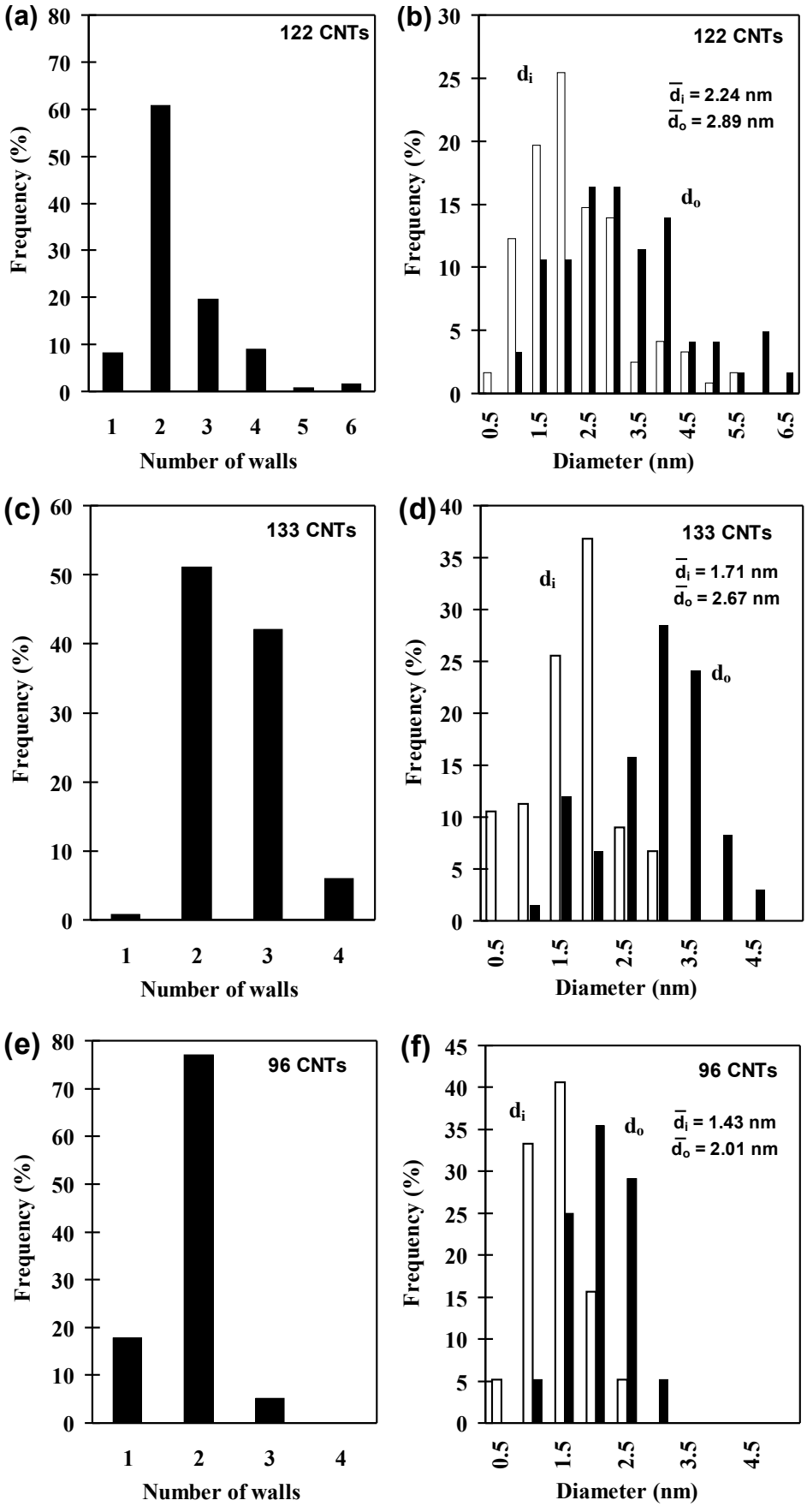
(a)
122 CNTs
Frequency (%)
Number of walls
(b)
122 CNTs
d_i
$\bar{d}_i$ = 2.24 nm
$\bar{d}_o$ = 2.89 nm
d_o
Frequency (%)
Diameter (nm)
(c)
133 CNTs
Frequency (%)
Number of walls
(d)
133 CNTs
d_i
$\bar{d}_i$ = 1.71 nm
$\bar{d}_o$ = 2.67 nm
d_o
Frequency (%)
Diameter (nm)
(e)
96 CNTs
Frequency (%)
Number of walls
(f)
96 CNTs
d_i
d_o
$\bar{d}_i$ = 1.43 nm
$\bar{d}_o$ = 2.01 nm
Frequency (%)
Diameter (nm)

FIGURE 6